

Supporting Information

Chalcogenide substitution in the [2Fe]-cluster of [FeFe]-hydrogenases conserves high enzymatic activity

Leonie Kertess^{a‡}, Florian Wittkamp^{b‡}, Constanze Sommer^{c‡}, Julian Esselborn^a, Olaf Rüdiger^c, Edward J. Reijerse^c, Eckhard Hofmann^d, Wolfgang Lubitz^c, Martin Winkler^a, Thomas Happe^{a*}, Ulf-Peter Apfel^{b*}

^a Ruhr-Universität Bochum, Lehrstuhl für Biochemie der Pflanzen, AG Photobiotechnologie, Universitätsstraße 150, 44801 Bochum

^b Ruhr-Universität Bochum, Anorganische Chemie I / Bioanorganische Chemie, Universitätsstraße 150, 44801 Bochum

^c Max-Planck-Institut für Chemische Energiekonversion, Stiftstraße 34-36, 45470 Mülheim an der Ruhr

^d Ruhr-Universität Bochum, Lehrstuhl für Biophysik, AG Röntgenstrukturanalyse an Proteinen, Universitätsstraße 150, 44801 Bochum

Table S1. H₂ production activities of Cpl-ADSe, HydA1-ADSe, Cpl-ADT and HydA1-ADT in [$\mu\text{mol H}_2$ per min per mg enzyme].

Table S2. H₂ production and uptake activities of Cpl-ADSe, HydA1-ADSe, Cpl-ADT and HydA1-ADT.

Table S3. Crystal data and structure refinement for 2a and 2b.

Table S4. Selected bond lengths and angles of 2a and 2b.

Table S5. Crystal data and refinement statistics.

Figure S1. Comparison of relative hydrogen evolution activity of fresh and stored Cpl-ADSe and HydA1-ADSe.

Figure S2. Oxygen exposure of Cpl-ADT, Cpl-ADSe, HydA1-ADT and HydA1-ADSe to air saturated buffer.

Figure S3. Transmission FT-IR spectra of Cpl-ADSe and HydA1-ADSe as thawed.

Figure S4. Transmission FT-IR spectra of free complexes in aqueous solution.

Figure S5. Gauss fits of overlapping CO bands of Cpl-ADSe and Cpl-ADT.

Figure S6. ORTEP representation of the asymmetric unit of $[\text{Fe}_2\{\mu(\text{SeCH}_2)_2\text{NCO}(\text{O})\text{CH}_2\text{Ph}\}(\text{CO})_6]$ (2a) and $[\text{Fe}_2\{\mu(\text{SeCH}_2)_2\text{NCO}(\text{O})\text{CH}_2\text{CH}_3\}(\text{CO})_6]$ (2b). Ellipsoids displayed at 50% probability.

Figure S7. X-ray fluorescence of the Cpl-ADSe crystal.

Figure S8. Model of the H-cluster of Cpl-ADSe.

Figure S9. The central cavity of Cpl-ADSe.

Figure S10. Cyclovoltammograms of Cpl and HydA1 matured with ADT and ADSe.

Figure S11. Chronoamperometry (CA) for the evaluation of oxygen sensitivity on HydA1-ADSe and HydA1-ADT.

Additional catalytic activity data

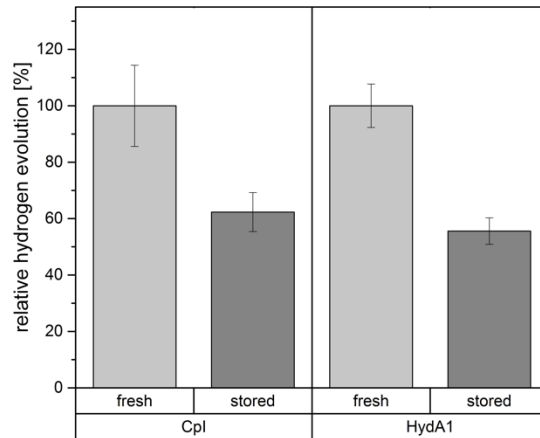


Figure S1. Comparison of relative hydrogen evolution activity of fresh and stored Cpl-ADSe and HydA1-ADSe. Initial activities represent values obtained just after *in vitro* maturation. For shelf life tests Cpl-ADSe sample was stored for 7 months at -80°C while and HydA1-ADSe was stored for 1 month at -80°C and thawed twice. Measurements were done in triplicates. Activity tests for methyl viologen dependent H_2 production was carried out in 100 mM $\text{K}_2\text{HPO}_4/\text{KH}_2\text{PO}_4$ buffer (pH 6.8), 10 mM methyl viologen with the addition of 100 mM sodium dithionite. Activities are presented relative to initial HydA1-ADT and Cpl-ADT activity (both set to 100 %). Error bars indicate standard deviation.

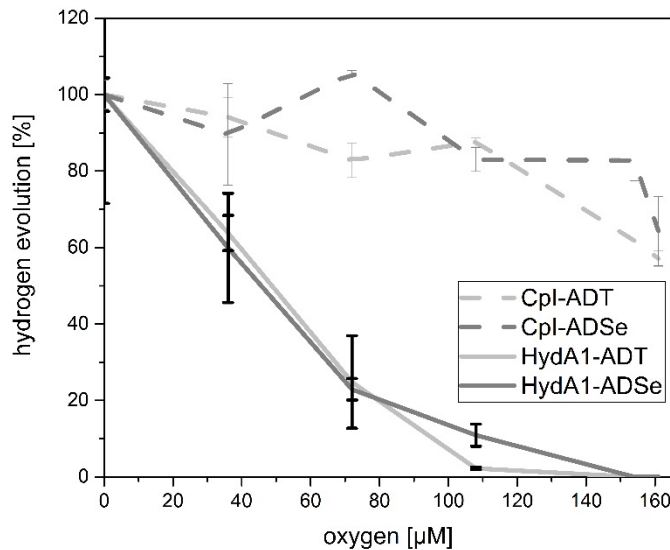


Figure S2. Oxygen exposure of Cpl-ADT, Cpl-ADSe, HydA1-ADT and HydA1-ADSe to air saturated buffer. Increasing amounts of air saturated buffer corresponding to 0 to 161 μM oxygen were added to 50 ng of *in vitro* matured hydrogenases and incubated for 5 min at RT in order to compare the influence of oxygen on Cpl-ADT, Cpl-ADSe, HydA1-ADT and HydA1-ADSe. Data was obtained from parallel measurements in duplicate. Initial activities of Cpl-ADT, Cpl-ADSe, HydA1-ADT and HydA1-ADSe were set to 100 %. Error bars indicate standard deviation.

Table S1. H₂ production activities of Cpl-ADSe, HydA1-ADSe, Cpl-ADT and HydA1-ADT in [$\mu\text{mol H}_2$ per min per mg enzyme]. Activity tests for methyl viologen dependent H₂ production was carried out in 100 mM K₂HPO₄/KH₂PO₄ buffer (pH 6.8), 10 mM methyl viologen with the addition of 100 mM sodium dithionite. Representative data of HydA1-ADSe and Cpl-ADSe from two independent preparations for at least two measurements in triplicates from samples analyzed by FT-IR spectroscopy in parallel.

[FeFe]-hydrogenase	ADSe	ADT
Cpl	1240 \pm 178	1453 \pm 225
HydA1	1198 \pm 93	983 \pm 82

Table S2. H₂ production and uptake activities of Cpl-ADSe, HydA1-ADSe, Cpl-ADT and HydA1-ADT. Activities given in [$\mu\text{mol H}_2$ per min per mg enzyme] using MV as electron mediator. Ratio of MV dependent H₂ uptake to H₂ production is given as ratio. Activity tests for MV dependent H₂ production were carried out in 100 mM K₂HPO₄/KH₂PO₄ buffer (pH 6.8), 10 mM MV with the addition of 100 mM NaDT. The activity tests for MV dependent H₂ uptake were carried out in 100 mM K₂HPO₄/KH₂PO₄ buffer (pH 6.8), 40 mM MV (HydA1) or 10 mM MV (Cpl) using 5 to 80 ng enzyme under 100 % H₂. H₂ production and uptake were determined on the same day from identical protein preparations.

Sample	H ₂ evolution [$\mu\text{mol H}_2$ per min per mg protein]	H ₂ uptake [$\mu\text{mol H}_2$ per min per mg protein]	Ratio uptake/evolution
Cpl-ADT	2335 \pm 86	410 \pm 47	17.6 $\times 10^{-2}$
Cpl-ADSe	1582 \pm 207	79 \pm 36	5.0 $\times 10^{-2}$
HydA1-ADT	728 \pm 5	281 \pm 3	38.6 $\times 10^{-2}$
HydA1-ADSe	199 \pm 62	19 \pm 3	9.5 $\times 10^{-2}$

It should be noted that for exact comparison of activities, ideally the same amount of protein and electron mediator should be used in the measurement, which, however, was not possible for the oxidation assays due to the diversity of activities and the need to stay within the linear range of the spectrometer. Since this analysis was done about one year after the initial measurements presented in Table S1, the overall higher hydrogen evolution activities might be reasoned by a different batch of chemicals and slight modifications in the detection method. However, the values reflect the same trends as seen before and are still within the range reported in literature.¹

Additional Spectroscopy Data

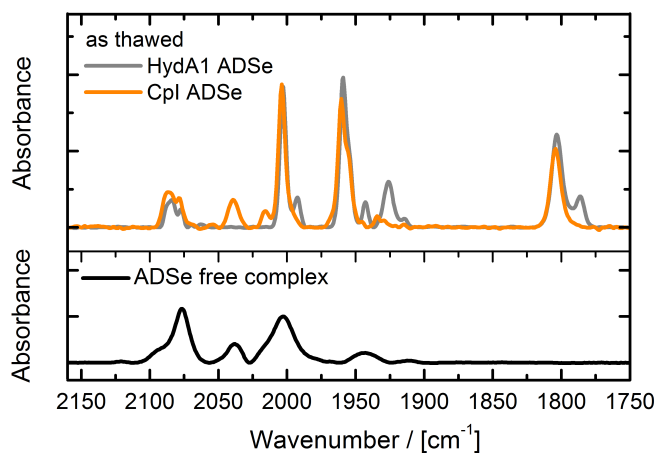


Figure S3. Transmission FT-IR spectra of Cpl-ADSe and HydA1-ADSe ($350 \mu\text{M}$) as thawed and ADSe free complexes. Samples were in 100 mM Tris-HCl, 150 mM NaCl (pH 8). Spectra were taken at 15°C with 2 cm^{-1} resolution.

The free ADSe complex in aqueous solution shows an IR pattern different from that of ADT. The shifts are rather large, suggesting that the complex adopts a different conformation. The observed bands for ADSe do not fit to any known ADT variants.²

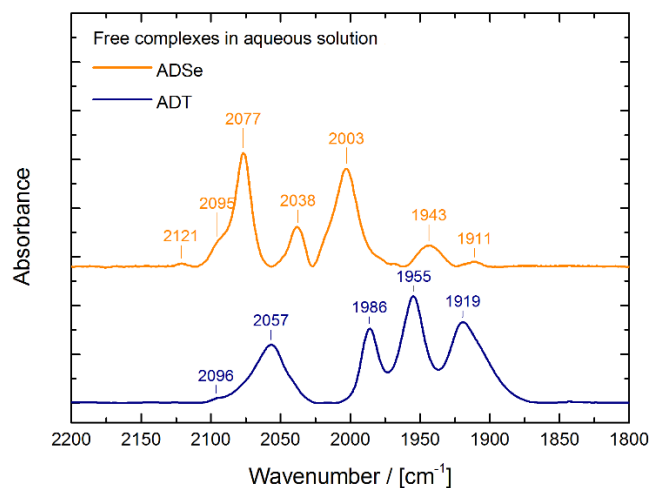


Figure S4. Transmission FT-IR spectra of free complexes in aqueous solution. ADSe complex in solution shows a blue shift compared to ADT in its CO and CN^- vibrations.

In the FTIR of Cpl-ADT as well as Cpl-ADSe (Figure 2) two CO vibrations strongly overlap. In Figure S5 these bands are deconvoluted using two Gaussian line shapes. For the fits following equations were used:

$$y = a \cdot \exp\left(\frac{-(x-x_0)^2}{2 \cdot b^2}\right) \quad (1)$$

$$\text{FWHM} = 2 \cdot \sqrt{2 \cdot \ln(2)} \cdot b \quad (2)$$

For Cpl-ADT the fits result in peak positions of 1974 and 1970 cm^{-1} which is consistent with the data reported in literature.³

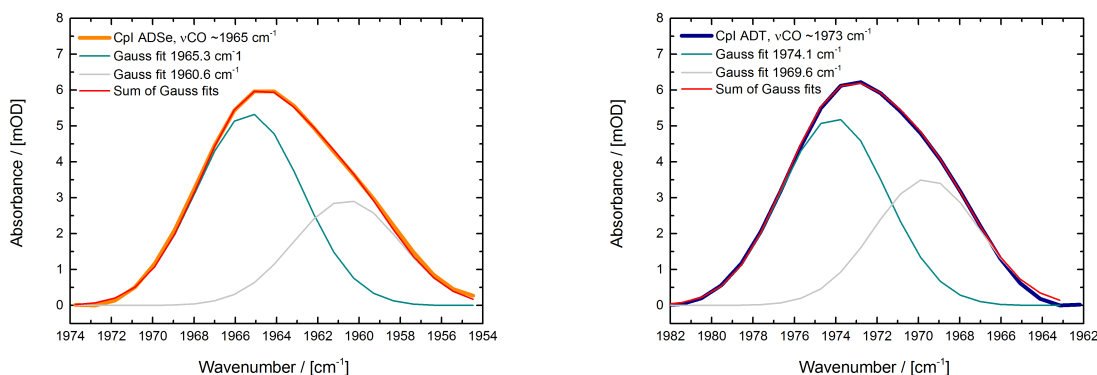


Figure S5. Gauss fits of overlapping CO bands of Cpl-ADSe (left) and Cpl-ADT (right). Left: Following parameters are used: 1965.3 cm^{-1} , $a_1= 5.35$ (corresponding to 64%); 1960.6 cm^{-1} , $a_2= 2.93$ with FWHM 6.0 for both fits. Right: 1974.1 cm^{-1} , $a_1= 5.23$ (60%), 1969.6 cm^{-1} , $a_2= 3.52$ with FWHM 6.0 each. Gauss fits are calculated in the same spectral resolution as the experimental spectra.

Additional Structural Data

Table S3. Crystal data and structure refinement for 2a and 2b.

Property	Value	
	2a	2b
Identification code		
Empirical formula	C ₂₄ HN ₁₃ O ₁₀ FeSe ₄	C ₁₁ H ₉ NO ₈ Fe ₂ Se ₂
Formula weight	614.88	552.81
Temperature/K	114(4)	111(1)
Crystal system	triclinic	monoclinic
Space group	P-1	P2 ₁ /n
a/Å	7.8537(2)	9.78531(10)
b/Å	9.3351(2)	8.65801(11)
c/Å	14.4434(4)	20.60799(20)
α/°	100.188(2)	90
β/°	100.216(2)	102.8436(10)
γ/°	100.918(2)	90
Volume/Å ³	998.70(5)	1702.25(3)
Z	2	4
ρ _{calc} /cm ³	2.0446	2.157
μ/mm ⁻¹	16.229	18.940
F(000)	589.9	1064.0
Crystal size/mm ³	0.1744 × 0.1349 × 0.1	0.23 × 0.1027 × 0.0791
Radiation	Cu Kα (λ = 1.54184)	CuKα (λ = 1.54184)
2θ range for data collection/°	9.88 to 152.36	8.802 to 152.814
Index ranges	-9 ≤ h ≤ 9, -11 ≤ k ≤ 11, -17 ≤ l ≤ 17	-12 ≤ h ≤ 12, -10 ≤ k ≤ 10, -25 ≤ l ≤ 25
Reflections collected	19982	25880
Independent reflections	4105 [R _{int} = 0.0249, R _{sigma} = 0.0164]	3540 [R _{int} = 0.0262, R _{sigma} = 0.0126]
Data/restraints/parameters	4105/0/261	3540/0/218
Goodness-of-fit on F ²	1.054	1.048
Final R indexes [I >= 2σ (I)]	R ₁ = 0.0236, wR ₂ = 0.0628	R ₁ = 0.0171, wR ₂ = 0.0420
Final R indexes [all data]	R ₁ = 0.0248, wR ₂ = 0.0633	R ₁ = 0.0181, wR ₂ = 0.0424
Largest diff. peak/hole / e Å ⁻³	0.61/-0.45	0.38/-0.47
CCDC reference	1570441	1570440

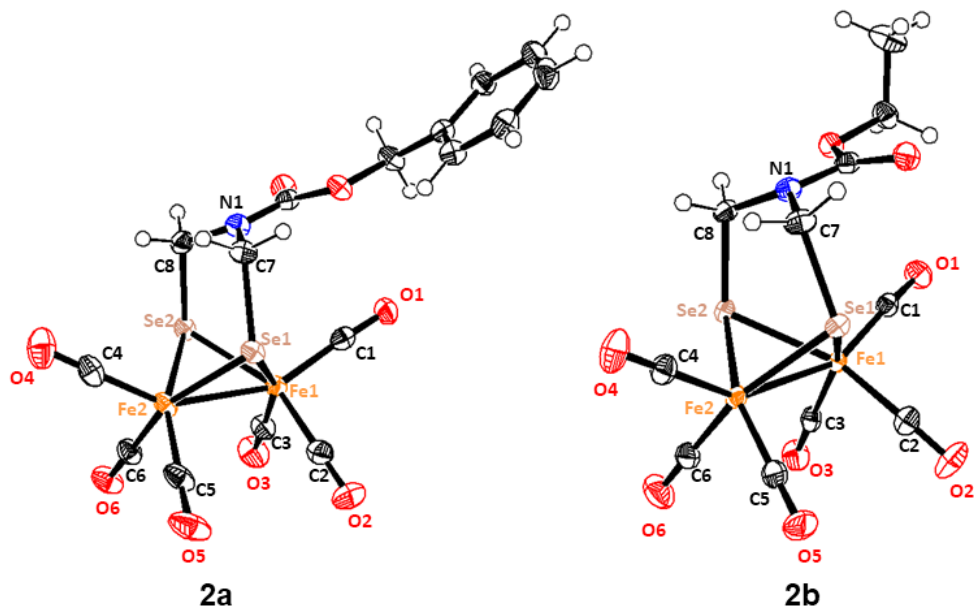


Figure S6. ORTEP representation of the asymmetric unit of $[\text{Fe}_2\{\mu(\text{SeCH}_2)_2\text{NCO}(\text{O})\text{CH}_2\text{Ph}\}(\text{CO})_6]$ (2a) and $[\text{Fe}_2\{\mu(\text{SeCH}_2)_2\text{NCO}(\text{O})\text{CH}_2\text{CH}_3\}(\text{CO})_6]$ (2b). Ellipsoids displayed at 50% probability.

Table S4. Selected bond lengths and angles of 2a and 2b.

Atoms	Bond length [Å] / Bond angle [°]	
	2a	2b
Fe1-Fe2	2.5405(5)	2.5296(4)
Fe1-Se1	2.3733(4)	2.3906(3)
Fe1-Se2	2.3859(4)	2.3765(3)
Fe2-Se1	2.3882(4)	2.3766(3)
Fe2-Se2	2.3768(4)	2.3901(3)
Se1-C7	2.008(2)	1.9946(18)
Se2-C8	1.996(2)	2.0058(17)
Se1-Fe1-Se2	87.063(13)	86.964(10)
Se1-Fe1-Fe2	58.040(11)	57.684(9)
Se2-Fe1-Fe2	57.591(12)	58.208(9)
Se1-Fe2-Fe1	57.471(11)	58.223(9)
Se1-Fe2-Se2	86.932(13)	86.964(10)
Se2-Fe2-Fe1	57.939(12)	57.689(9)
Fe1-Se1-Fe2	64.489(12)	64.093(10)
Fe1-Se2-Fe2	64.471(13)	64.103(10)

Table S5. Crystal data and refinement statistics.

Property	Value
Wavelength (eV)	12644
Space group	P 1 2 ₁ 1
Unit cell parameters	90.35 72.88 103.10
a, b, c, α , β , γ	90.0 98.7 90.0
Resolution range (Å)	47.50 - 2.05 (2.10 - 2.05) ^a
Total reflections	615226 (46457)
Unique reflections	162396 (12146)
Multiplicity	3.78843 (3.8248)
Completeness (%)	99.5 (99.7)
R_{meas} (%)	16.9 (119.9)
$I/\sigma(I)$	7.15 (1.50)
CC 1/2	99.3 (72.3) ^b
Resolution (Å)	2.05
R_{work}	0.2321 (0.3328)
R_{free}	0.2685 (0.3757)
No. atoms (except H)	9760
Protein	8933
Ligand	106
Solvent/ion	716/5
RMSD from ideal bond lengths (Å)	0.004
RMSD from ideal bond angles (°)	0.59
Ramachandran favored (%)	96.0
Ramachandran allowed (%)	4.0
Ramachandran outliers (%)	0.0
Clashscore	1.12
Average B factor	39.10
Wilson B factor (Å ²)	27.07

^a Numbers in the parenthesis represent values for the highest resolution bin.

^b Correlation coefficient CC 1/2 as defined in Karplus and Diederichs, 2012.⁴

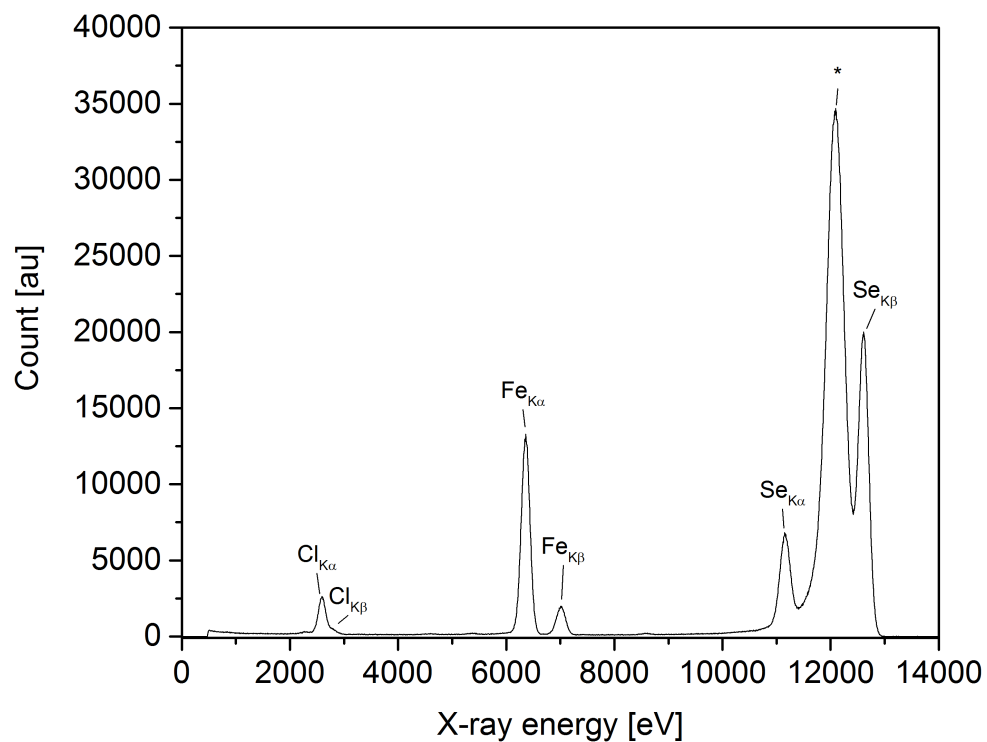


Figure S7. X-ray fluorescence of the Cpl-ADSe crystal. Excitation at 12656 eV. * indicates back-scattering.

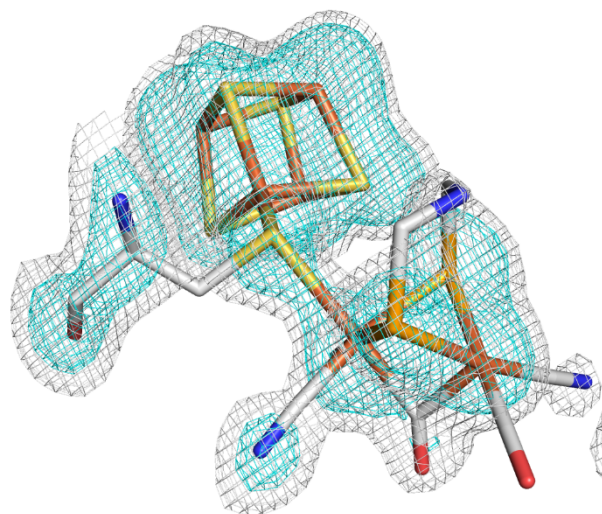


Figure S8. Model of the H-cluster of Cpl-ADSe. Stick model of Cpl-ADSe (PDB 50EF) $F_o - F_c$ simulated annealing omit map contoured at 1.5 (cyan) and 3.5 (grey) σ .

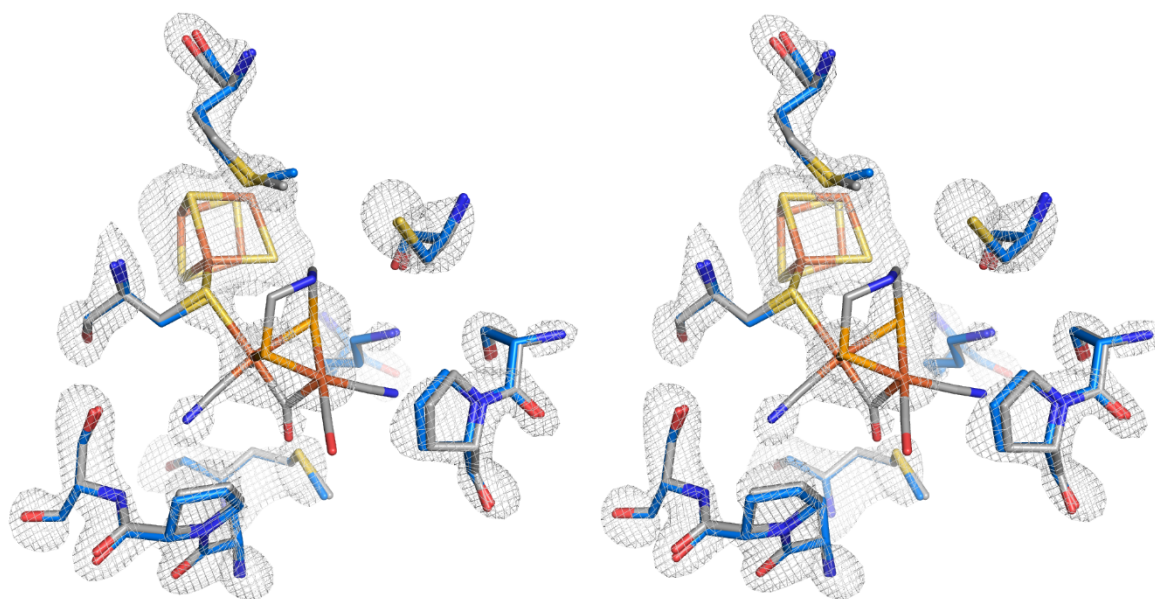


Figure S9. The central cavity of Cpl-ADSe. Stereo view of a stick model of the central cavity of Cpl-ADSe (PDB 5OEF; carbon atoms in grey) with $F_o - F_c$ simulated annealing omit map contoured at 3.0σ . A stick model of amino acids lining the central cavity of Cpl-ADT is superposed (PDB 4XDC; carbon atoms in marine).

Additional electrochemistry data

Direct comparison on the absolute currents revealed that for Cpl-ADSe the catalytic current for hydrogen production is 10 fold less than for Cpl-ADT. For HydA1-ADSe the current is about three times less.

For electrochemistry experiments it was inevitable to freeze and thaw the samples. To test if a further freeze/thaw cycle leads to an additional loss of activity, further CVs were recorded. However, no further loss in activity was found. In solution, a similar behavior after storage of ADSe samples was observed. Eventually, CO inhibition of the enzyme during storage protects a fraction of the sample from degradation and upon CO release under catalytic conditions this fraction displays full activity.

It should be kept in mind that the comparison of the absolute magnitude is meaningless due to the unknown electroactive coverage on the electrode. However, the ratio of the oxidation over reduction currents can be used to reveal a bias to either direction compared to the WT as done in our study.⁵

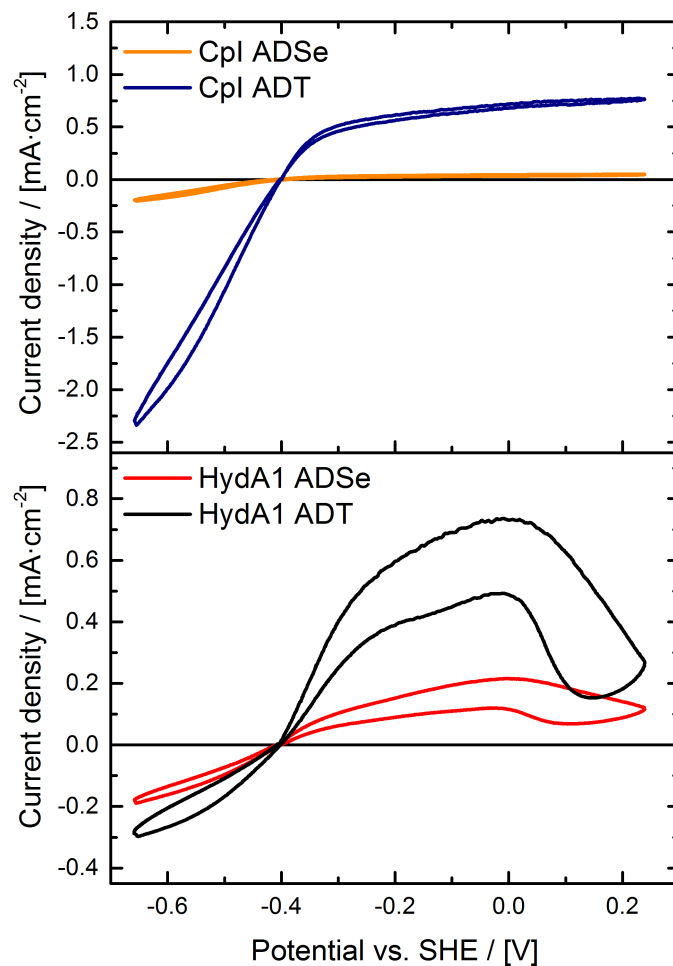


Figure S10. Cyclic voltammograms of Cpl and HyDA1 maturated with ADT and ADSe. Samples were thawed, diluted to 3 μM (10 mM MES, 2 mM NaDT, pH 5.8) and adsorbed to the PG electrode. Measurements are carried out at 25°C, 100 % H₂ with 20 mV/s scan rate, electrode rotation of 2000 rpm in buffer at pH 7.0.

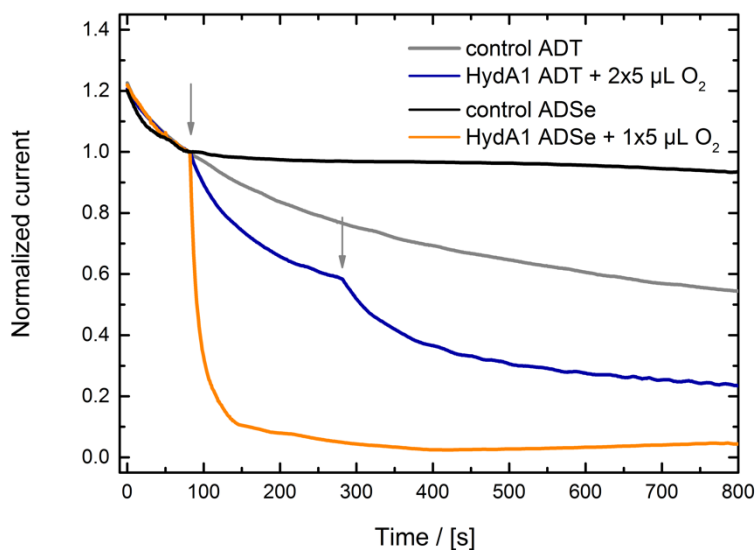


Figure S11. Chronoamperometry (CA) of HydA1-ADSe and HydA1-ADT upon addition of O₂ saturated buffer to compare their level of oxygen sensitivity. Currents were normalized to the value just before the first O₂ addition. Each arrow indicates the addition of 5 µL O₂ saturated buffer to a total volume of 5 mL, respectively. CA was recorded at -39 mV vs. SHE, 25°C, 100% H₂, pH 7.0 and during an electrode rotation of 2000 rpm. Individual protein films were used for the oxygen exposed and control experiments.

1 Esselborn *et al.*, *Nat. Chem. Biol.*, 2013, 9, 607–609.

2 J. F. Siebel, A. Adamska-Venkatesh, K. Weber, S. Rumpel, E. Reijerse and W. Lubitz, *Biochemistry*, 2015, 54, 1474–1483.

3 Z. Chen, B.J., Lemon, S. Huang, D.J. Swartz, J.W. Peters and K.A. Bagley, *Biochemistry*, 2002, 41, 2036–2043.

4 P. A. Karplus and K. Diederichs, *Science*, 2012, 336, 1030–1033.

5 A. Abou Hamdan, S. Dementin, P.-P. Liebgott, O. Gutierrez-Sanz, P. Richaud, A.L. De Lacey, M. Rousset, P. Bertrand, L. Cournac and C. Léger, *J. Am. Chem. Soc.*, 2012, 134, 8368–8371.